PCCP

Accepted Manuscript

This is an *Accepted Manuscript*, which has been through the Royal Society of Chemistry peer review process and has been accepted for publication.

Accepted Manuscripts are published online shortly after acceptance, before technical editing, formatting and proof reading. Using this free service, authors can make their results available to the community, in citable form, before we publish the edited article. We will replace this *Accepted Manuscript* with the edited and formatted *Advance Article* as soon as it is available.

You can find more information about *Accepted Manuscripts* in the Information for Authors.

Please note that technical editing may introduce minor changes to the text and/or graphics, which may alter content. The journal's standard Terms & Conditions and the Ethical guidelines still apply. In no event shall the Royal Society of Chemistry be held responsible for any errors or omissions in this *Accepted Manuscript* or any consequences arising from the use of any information it contains.

ROYAL SOCIETY OF CHEMISTRY

www.rsc.org/pccp

Molecular dynamics investigations of liquid-vapor interaction and adsorption of formaldehyde, oxocarbons, and water in graphitic slit pores

Pei-Hsing Huang[1,*], Shang-Chao Hung[2], Ming-Yueh Huang[1]

[1]*Department of Mechanical Engineering, National Pingtung University of Science and Technology, Pingtung 912, Taiwan, Republic of China*
[2]*Department of Information Technology & Communication, Shih Chien University Kaohsiung Campus, Neimen, Kaohsiung 845, Taiwan, Republic of China*

Abstract   Formaldehyde exposure has been associated with several human cancers, including leukemia and nasopharyngeal carcinoma, motivating the present investigation on the microscopic adsorption behaviors of formaldehyde in multi-component-mixture-filled micropores. Molecular dynamics (MD) simulation was used to investigate the liquid-vapor interaction and adsorption of formaldehyde, oxocarbons, and water in graphitic slit pores. The effects of slit width, system temperature, concentration, and constituent ratio of the mixture on the diffusion and adsorption properties are studied. As a result of interactions between the components, the z-directional self-diffusivity (D_z) in the mixture substantially decreased by about one order of magnitude as compared with that of pure (single-constituent) adsorbates. When the concentration exceeds a certain threshold, the D_z values dramatically decrease due to over-saturation inducing barriers to diffusion. The binding energy between the adsorbate and graphite at the first adsorption monolayer are calculated to be 3.99, 2.01, 3.49, and 2.67 kcal/mol for CO_2, CO, CH_2O, and H_2O, respectively. These values agree well with those calculated using the density functional theory coupled cluster method and experiment results. A low solubility of CO_2 in water and water preferring to react with CH_2O, forming hydrated methanediol clusters, are observed. Because the cohesion in a hydrated methanediol cluster is much higher than the adhesion between clusters and the graphitic surface, the hydrated methanediol clusters were hydrophobic, exhibiting a large contact angle on graphite.

---

[*]Corresponding author. E-mail address: phh@mail.npust.edu.tw (P.-H. Huang)

1. Introduction

The application of porous materials for the adsorption of harmful fluids and greenhouse gases has attracted extensive research interest.[1-16] However, most studies have focused on the performances of the adsorbents, especially in terms of the adsorbed number of molecules, without expounding why and how adsorption and separation occur at the atomistic scale.[1] Consequently, many microscopic mechanisms of intermolecular interaction in this domain are still not fully known, such as the behavior of fluid adsorption in micropores for pore sizes with molecular dimensions. Such small systems are experimentally inaccessible but quite important in diverse applications, such as chromatography, waste water recovery, and membrane separation technologies.[2,3] It is thus desirable to establish a flexible molecular model so as to predict the ideal adsorption conditions, and to investigate atomic-scale sorption phenomena and properties in complex fluid-filled pores.

The development of highly efficient, reversible, and cost-effective adsorption technologies is of fundamental and practical interest for environmental amelioration. Selective adsorption in microporous materials is simple and promising for separating a particular component from a pollutant stream before it is emitted into the environment. The selectivity can be effectively regulated by a number of parameters, such as interactions between adsorbate molecules (e.g., diffusivity ratio[3], polarization, and H-bonding[4,11]), surface properties of the adsorbent (e.g., surface-activated[5] or hydrophilic/hydrophobic[6]), pore conformation (e.g., size[2,8] and shape[15]), and adsorption conditions (e.g., concentration[4,7], constituent[4,16], temperature[7,10], and pressure[1,3]). By optimizing the material parameters and manipulating adsorption at specific thermodynamic conditions, one can significantly promote selectivity by many orders of magnitude.[4,5] Therefore, thoroughly understanding the various adsorption and diffusion properties of fluid mixtures adsorbed in micropores is crucial.

Microporous materials have been demonstrated to have outstanding capabilities for capturing various specific molecules. Kapoor and Yang[3] used molecular sieve

carbons as the adsorbent and obtained a diffusivity ratio for CO_2/CH_4 of 180 at 298 K. The difference in diffusivities was applied for kinetic separation. The cycle time was chosen to allow significant sorption of CO_2 but preclude CH_4 from entering the micropores. Wan and Ju[4] investigated the behavior of ethanol and water mixtures inside Au nanotubes. The distributive probability and number of H-bonds affected molecular adsorption conformations and adsorption behaviors of the mixtures in the nanotubes. Shevade et al.[5] investigated the adsorption behavior of methanol-water mixtures in activated carbon (AC) micropores using grand canonical Monte Carlo (GCMC) simulations. They calculated salvation forces as a function of pore size. The negative salvation forces reflected the hydrophilic interaction of the mixtures with the AC surfaces. Heuchel et al.[8] studied the adsorption of CO_2 and CH_4 mixtures in a slit-shaped AC using GCMC simulations. The AC contained a great number of pores small than 6.1 Å. These pores are accessible only to CO_2, and they are therefore responsible for a partial molecular sieving effect in the mixture adsorption. Vishnyakov et al.[9] studied CO_2 adsorption in graphite (GR) micropores at 273 K using GCMC simulations and density functional theory (DFT). An effective Lennard-Jones (L-J) model for DFT was developed to calculate the isotherms of CO_2 adsorption on GR at 273 and 195 K. Ballenegger et al.[10] reported the diffusion process of CH_2O in proton-disordered ice in the temperature range of 200~273 K. They observed that CH_2O molecules diffused in ice predominantly by jumping between B sites (centers of O-O bond) via the bond-breaking mechanism. Collignon and Picaud[11] studied the adsorption of CH_2O and CH_3OH on proton-disordered ice surfaces at 210 and 250 K. They concluded that the adsorption of CH_3OH is governed by its ability to form hydrogen bonds with the ice surface, which leads to large adsorption energy values. Bhatia et al.[12] investigated the adsorption capacity and behaviors of CO_2 in GR slit pores using a single-center L-J and three-center potential model incorporating local charges. They concluded that the single-center LJ approximation is inadequate to account for the structure of linear molecules such as CO_2 in narrow pores. Liu and Smit[13] evaluated the separation performance of two

typical zeolitic imidazolate frameworks for CO_2/N_2, CO_2/CH_4, and CH_4/N_2 mixtures. They concluded that electrostatic interactions are a key factor in the adsorption selectivity. Liu *et al.*[14] studied CO_2 adsorption, decomposition, and reduction via transition metal (Fe, Co, Ni, and Cu) surface catalysts using DFT calculations. Skarmoutsos *et al.*[15] designed a three-dimensional porous nanotube network to enhance CO_2 adsorption selectivity in an equimolar CO_2/N_2 mixture. Zhou and Wang[16] investigated the adsorption and diffusion of supercritical CO_2 in slit pores. They found that diffusion coefficients of CO_2 molecules confined in a slit pore in supercritical conditions strongly depend on the pore fluid density.

The aforementioned research gives comprehensive insight into the adsorption characteristics of AC, GR, and related adsorbents. Nevertheless, most of the studies focused on the adsorption of single-component or binary mixtures under specific thermodynamic conditions. Few systematic empirical or theoretical studies have been conducted on the interaction of multi-component mixtures or the sieving of a specific molecular group from a multi-component mixture. In actuality, environment system or pollutants are mostly multi-component hybrids, some which operate under supercritical thermodynamic conditions[16]. Formaldehyde exposure has been associated with several human cancers, including leukemia and nasopharyngeal carcinoma, motivating the present investigation on the microscopic adsorption behaviors of formaldehyde in multi-component-mixture-filled micropores. Carbon monoxide, carbon dioxide, and water vapor are the most common toxic byproducts and greenhouse gases generated by fossil-fuel-related processes and modern industries. These molecules commonly blend in the atmosphere and affect human health and the warming effect. A $CH_2O/CO/CO_2/H_2O$ mixture with various mole fractions inside a GR slit pore is thus investigated in this work. To ensure model adequacy for the study of dynamic adsorption processes and interactions between intermolecular clusters, a fully atomistic molecular dynamics modeling approach is adopted. Several distinct objectives of this study include (i) the mechanisms of incipient pile up and eventual adsorption conformation for pure CH_2O, CO_2, CO,

H_2O, and their mixtures confined in GR slit pores, (ii) how to enhance interfacial binding strength between adsorbates and the GR surface via regulating the composition ratio of mixtures, (iii) the effects of thermodynamic conditions on the static adsorption, self-diffusivity, and adsorption isotherm, and (iv) the roles of the water, formaldehyde, and oxocarbons in the interfacial wetting and electrochemical properties of mixtures.

2. Models and Computational Details

The dynamic adsorption behaviors of CH_2O, CO_2, CO, and H_2O mixtures in the GR basal slits were investigated using MD simulation in the isothermal-isochoric (NVT) ensemble. In order to simulate this system accurately, the energy calculation and dynamics (ENCAD) force field[17,18] and the L-J combined Coulomb pair potentials[5,19-23] were employed to model full-atomistic interactions in the present study. The ENCAD potential model not only accurately depicts the molecular structure detected by X-ray diffraction and nuclear magnetic resonance, but also yields trajectories of the structural and dynamic properties corresponding with those obtained from experimental data.[17] The complete form of the ENCAD potential model used here is expressed as follows:

$$U_{tot} = U_{bond\ length} + U_{bond\ angle} + U_{nonbonded} \tag{1}$$

where $U_{bond\ length}$ and $U_{bond\ angle}$ describe the potential energies regarding the stretching and bending, respectively, of the covalent bonds for CO_2, CO, CH_2O, and H_2O molecules. The two potential functions are given by:

$$U_{bond\ length} = \sum_{i}^{bonds} \frac{1}{2} k_b^i (b_i - b_0^i)^2 \tag{2}$$

$$U_{bond\ angle} = \sum_{i}^{bond\ angles} \frac{1}{2} k_\theta^i (\theta_i - \theta_0^i)^2 \tag{3}$$

where K_b^i and K_θ^i are force constants representing the bond stretching and bond bending barrier of the ith bond, respectively; b_i, θ_i, b_0^i, and θ_0^i denote the ith bond length, the ith bending angle, the equilibrium length of the ith bond, and the

equilibrium angle of the ith bending angle, respectively. The parameters used for describing the bond length energy and bond angle energy are summarized in Table 1. The last term in Eq. (1) describes nonbonded interactions, including the van der Waals and electrostatic potentials, which represent the interactions between pairs of atoms separated by different molecules or covalent structures. This work adopts a flexible three-centered (F3C) water model based on the ENCAD potential to describe the interactions between water molecules.[18] For the nonbonding pair of interacting atoms i and j in the water nanocluster with an interatomic distance r_{ij}, the van der Waals potential (U_{vdw}) and electrostatic potential (U_{els}) can be respectively expressed as:

$$U_{vdw} = \sum_{nonbonded\ pairs} [A_{SC}\varepsilon(\frac{r_0}{r_{ij}})^{12} - 2\varepsilon(\frac{r_0}{r_{ij}})^6 - S_{vdw}^A(r_{ij})] \tag{4}$$

$$U_{els} = \sum_{pairs} 332[q^i q^j / r_{ij} - S_{els}^A(r_{ij})] \tag{5}$$

The parameter A_{sc} in Eq. (4) is a scale factor used to compensate for the reduced attraction caused by the truncation of potential energy. The A_{sc} value depends on the cutoff distance, r_c. The optimum values were derived by Levitt et al.[18] Here, the suggested value of $A_{sc} = 0.84$ associated with a cutoff distance $r_c = 6$ Å is adopted. The term $S_{vdw}^A(r_{ij})$ in Eq. (4) and the term $S_{els}^A(r_{ij})$ in Eq. (5) represent the truncation shift functions of the van der Waals and electrostatic potentials, respectively. The truncation shift function has the general form:[18]

$$S_f^A(r) = \begin{cases} [f(r_c) + (r - r_c)(df(r_c)/dr)] & for\ r \leq r_c \\ 0 & for\ r > r_c \end{cases} \tag{6}$$

where $f(r_c)$ and r_c denote the energy function and the truncation distance, respectively. Accordingly, the complete forms of $S_{vdw}^A(r_{ij})$ and $S_{els}^A(r_{ij})$ can be obtained from Eq. (6) as:

$$S_{vdw}^A(r_{ij}) = [A_{SC}\varepsilon(\frac{r_0^{ij}}{r_c})^{12} - 2\varepsilon(\frac{r_0^{ij}}{r_c})^6] - \frac{12(r_{ij} - r_c)}{r_c}[A_{SC}\varepsilon(\frac{r_0^{ij}}{r_c})^{12} - \varepsilon(\frac{r_0^{ij}}{r_c})^6] \tag{7}$$

$$S_{els}^{A}(r_{ij}) = \frac{q^i q^j}{r_c} - (r_{ij} - r_c)\frac{q^i q^j}{r_c^2} \tag{8}$$

where q^i and q^j denote the partial charges of the oxygen or hydrogen atoms of two water molecules within the truncation distance. The nonbonded energy parameters used for water-water interactions in the F3C model[18] are given in Table 2. In order to make the simulations more efficient, simple potentials based on the L-J combined Coulomb pair potentials were adopted to model the nonbonded interactions between different molecules and the GR slit pores.[5,19-23] This potential model allows taking into account a large truncation distance to treat the nonbonded interactions between hetero-molecular clusters, which can be expressed as:

$$U_{nonbonded} = \sum_{i,j\ pairs}^{n_s} \frac{q_i q_j}{r_{ij}} + \sum_{i,j\ pairs}^{n_s} 4\varepsilon_{ij}[(\frac{\sigma_{ij}}{r_{ij}})^{12} - (\frac{\sigma_{ij}}{r_{ij}})^6)] \tag{9}$$

The first term in Eq. (9) denotes the long-range electrostatic interactions between different molecules, and the second term represents the short-range dispersion and repulsion interactions. n_s is the number of atomic pairs within the truncation distance r_c=15 Å. Regarding the interactions of a hetero-atomic pair, the effective values of σ and ε can be derived from those for the homo-atomic pairs using the standard Lorentz-Berthelot combining rules. The potential parameters used in Eq. (9) for various molecules are listed in Table 3.

The GR slits have lateral dimensions of 115.02 × 113.16 Å in the x and y directions and various slit widths (d) in the z direction. Various slit widths (d = 26.05, 37.44, 48.84, 60.24, 71.64, and 83.03 Å) were adopted for investigating the slit size effects, in which the slit width was calculated as the center-to-center distance of carbon atoms on opposing GR surfaces. Each slit wall consists of three layers of immobile GR. In each layer, the carbon atoms are arranged in a honeycomb lattice with a separation of 1.42 Å, and the distance between layers is 3.348 Å. The total number of carbon atoms in each slit wall is 14904. To simulate an infinite slit surface, periodic boundary conditions and the minimum imaging criterion[24] were adopted by replicating the simulation domain along the x and y directions. The GR slit contains a

certain number of adsorbate molecules that depends on the simulated molar concentrations (c_i), ranging from 1.128 to 3.38 mol/L. To avoid the artificial effect, the adsorbate molecules were well mixed inside the slit at the beginning of the simulations. For understanding the influences of constituent fraction on the adsorption behaviors of multi-component mixtures, mixtures comprising various mole fractions were systematically examined, as shown in Table 4. The mole fraction x_i is defined as the amount of a constituent n_i divided by the total amount of all constituents in a mixture n_{total} (i.e., $x_i = n_i / n_{total}$). As shown in Table 4, equimolar fractions (25%: 25%: 25%: 25%) for CO_2, CO, CH_2O, and H_2O were assigned in case I. In the other cases, one of the constituents was decreased in turn by 18.7%, 12.79%, and 6.25%, with other three constituents equally divided for the remaining fraction.

Before the simulations were conducted, the adsorbate molecules were well mixed inside the slit. Atoms in the system were randomly assigned velocities appropriate for the simulation temperature according to the Maxwell-Boltzmann distribution. The atoms were then allowed to act in accordance with Newton's equations of motion. The atomic positions, velocities, and accelerations, and intermolecular forces were derived in each computational time step of $\Delta t_{MD} = 1$ fs. The system was adequately thermally equilibrated at the desired temperature using the velocity rescaling method for 1 ns (i.e., one million time steps). Gear's fifth-order predictor-corrector algorithm[24] was employed to derive the trajectories of atoms. This algorithm has great flexibility and good stability, and also offers a good compromise between precision and computational time.[25,26]

3. Results and discussion

Figures 1(a)-(d) show the eventual adsorption conformations of formaldehyde, carbon dioxide, carbon monoxide, and water molecules, respectively, inside the GR slit with $d = 48.84$ Å and $c_i = 3.38$ mol/L at room temperature. The simulations were performed until the adsorptive process approached a statistical equilibration (~3 ns), i.e., the number of adsorbed molecules on the GR surface was close to being a

constant. The adsorption conformations of the four adsorbates are significantly distinct. In Fig. 1(a), the CH_2O molecules are almost entirely adsorbed to the GR surface except for a few suspended in the slit space. In contrast, a substantial number of CO_2 and CO molecules were not adsorbed but suspended in the slit space, with CO_2 molecules tending to aggregate (Fig. 1(b)) and CO molecules being greatly dispersed (Fig. 1(c)).

The wetting behaviors of water on a GR surface reported in previous experimental works[6,27,28-32] have a large variation, ranging from strongly hydrophilic (highly wettable) to hydrophobic (non-wettable), i.e., $0° \leq \theta_c \leq 94.2°$, where θ_c is the contact angle, providing an inverse measure of wettability. Li et al.[6] and Schrader[28,31] ascribed the higher contact angles previously reported[29,30] to impurities on the surface, such as chemisorption of hydrogen or hydrocarbon contamination from ambient air. In addition, θ_c values obtained from previous computational simulations[27,32-37] have been reported in a wide range of $0°$ to $127°$. This variation in simulation results can be ascribed to four main causes, namely (i) different potential energy parameters were employed to treat the water-water (i.e., cohesion) and water-GR (i.e., adhesion) interactions, (ii) different shapes of water droplet were adopted in the initial physical model (e.g., spherical[27,33,34,36] and cylindrical droplets[32,27], cubes[35], and slab film[37]), (iii) simulation scale and size (i.e., the number of water molecule and graphitic layers), and (iv) the eventual adsorptive conformation of the water droplet is not perfectly spherical and symmetric, and thus contact angles can largely change with viewpoint. Please note that in the physical model used in the present work, the water vapors is distributed uniformly inside a GR slit, i.e., not a 'liquid droplet' on a 'single' GR surface, which is entirely different from those in the aforementioned works. The water vapor is eventually adsorbed and condenses in the GR slit, forming dropwise films that are bridged by slender molecular chains across the slit space, as shown in Fig. 1(d).

3.1 Effect of slit width on dynamic diffusion and adsorption capacity

For understanding the microscopic mechanism of these molecular conformations,

the dynamic diffusion behaviors of adsorbates were further investigated. The molecular self-diffusivity can be determined either from Green-Kubo formulas, in which the velocity autocorrelation function is integrated over time, or from Einstein relations, in which the mean-square displacement (MSD) is differentiated with respect to time.[2,24,38] From a macroscopic perspective, because the separation of slit walls is finite, the self-diffusivity in the direction perpendicular to the slit walls should approach zero at long simulation times. However, considering the adsorbate molecules adsorbed to the slit walls, it is evident that the diffusion motions normal to the slit walls are more strongly affected by the confinement of the slits than are the motions parallel to the slit walls. The self-diffusivity coefficient in the z direction (D_z) in terms of molecular scale is therefore of interest and importance in the analysis. The Einstein relation:

$$D_z(t) = \lim_{t \to \infty} \frac{1}{N} \sum_{i=1}^{N} \left\langle \frac{\left| r_{i,z}(t) - r_{i,z}(0) \right|^2}{2t} \right\rangle \tag{10}$$

is used as a measure of the diffusion behavior in the direction perpendicular to the slit walls, where $r_{i,z}(t)$ and $r_{i,z}(0)$ are the z position of a tagged particle i at times t and 0, respectively. N denotes the total particle number and the angular bracket indicates an ensemble average. The value of D_z as a function of slit width for pure CH_2O, CO_2, CO, H_2O, and their mixtures are shown in Fig. 2. The simulations were performed with the concentration $c_i = 3.38$ mol/L at room temperature. As shown, the D_z of CO molecules increased sharply with increasing slit width. This phenomenon can be ascribed to the electrostatic potentials between CO molecules being very weak, less than one-hundredth the magnitude of the other studied adsorbates. The weak CO-GR interactions resulted in the CO molecules free diffusing and dispersing in the slit. CO_2 exhibited the lowest D_z value among the studied adsorbates, i.e., $1.1 \sim 3.0 \times 10^{-9}$ $m^2 \cdot s^{-1}$. The value is approximately that of a typical micropore fluid, which is on the order of 10^{-9} $m^2 \cdot s^{-1}$.[15,16] Since long-range CO_2-GR attraction is weaker than the attraction between CO_2 molecules, only the CO_2 molecules close to the GR walls could be adsorbed, with the remaining CO_2 being aggregated in the slit space. These

mechanisms result in a quick adsorption equilibrium and a small D_z value for pure CO_2.

Figure 2 shows that the D_z value of CH_2O changed with slit width. The high D_z values of CH_2O can be attributed to the van der Waals attractions between CH_2O and GR and the strong electronic attractions between CH_2O molecules. Consequently, the CH_2O molecules were almost completely adsorbed to the GR surface (Fig. 1(a)). The D_z values of H_2O ranged from 3.7 to 18.0 $\times 10^{-9}$ $m^2 \cdot s^{-1}$ for various slit widths, which are comparable with the experimental result of 2.6×10^{-9} $m^2 \cdot s^{-1}$.[39] The simulation results indicate that the water molecules in the fresh GR slit were hydrophilic, forming monolayer dropwise films that adhered on the GR walls, as shown in Fig. 1(d). This result contradicts the long-held impression that GR is a hydrophobic material. Li et al[6] showed that exposure to air-born hydrocarbons and contaminants makes GR surfaces hydrophobic. Their findings indicate that GR surfaces are more hydrophilic than previously believed. This idea was rechecked using molecular simulations in this work. The adsorption conformations for mixtures composed of various fractions of CH_2O, CO_2, CO, and H_2O molecules were investigated. As shown in Fig. 3(a), the few CO_2 molecules that dissolved in water were converted to carbonic acid. Many water molecules reacted with CH_2O molecules to form hydrate methanediol clusters instead of spreading on the GR surface. Due to the oxygen of water having a higher partial atomic charge than that of CH_2O (see Table 3), the globular clusters self-assembled into the H_2O-core and CH_2O-shell structure, as shown in Fig. 3(b). The hydrated structures are encircled by hydrogens of hydrate methanediol in the outermost layer. Since the van der Waals attraction between the outermost hydrogen and GR surfaces is much lower than H-bond strength and the hydration cohesion in clusters, the hydrated methanediol clusters were hydrophobic, exhibiting a large contact angle on GR. Apart from the results of computational simulations[40-42], some experimental investigations have reported the reaction and formation mechanisms of methanediol, i.e., the hydrated form of formaldehyde[42-47]. The hydrated reactions depend on the reaction temperature and the

concentration ratio of CH_2O/H_2O[42]. Moreover, the hydrated methanediol clusters can be generated by the infrared laser resonant desorption technique from frozen aqueous solutions of formaldehyde[43-45]. The cluster formation mechanism could be correlated with the presence of oligomers in the original liquid solution[46]; their presence in the solid phase has been recently confirmed by micro-Raman spectrometry[47].

The number of adsorbed molecules is another important index of the performance of an adsorbent. However, it is difficult to accurately determine the number of all adsorbed molecules due to various molecule-surface interactions (including short-lived adsorption, desorption, and reunion) at a time scale faster than several hundred femtoseconds. Here, a statistical index, i.e., the amount of static adsorption (N_{sa}), is used to quantify the adsorbed molecules. When the binding energy (E_b) approached ~ 0.5 kcal/mol, i.e., about one-tenth of the H-binding enthalpy in water, the molecules were in a steady adsorption state on GR. Since oxygen and carbon atoms are the common elements in CH_2O, CO_2, CO, and H_2O, the binding energy of oxygen-GR or carbon-GR interaction (i.e., $\left|E_b^{O-GR}\right|$ or $\left|E_b^{C-GR}\right| \geq 0.5$ kcal/mol) was calculated to determine whether a molecule was adsorbed. Figure 4 shows the changes of N_{sa} as a function of slit width for pure CH_2O, CO_2, CO, H_2O, and their mixtures. The simulations were performed at an equimolar concentration with $c_i = 3.38$ mol/L, i.e., the total number of molecules increased with slit width. As shown, N_{sa} sharply increased with increasing slit width for pure CH_2O and H_2O but only slightly increased for pure CO_2 and CO. The reason is the same as that for self-diffusivity given in the previous section. Of note, the N_{sa} and D_z values of the mixtures were almost constant with slit width. The major cause is that the formations of hydrate methanediol clusters and the blockades of CO_2 resulted in the highly diffusive CH_2O and H_2O molecules becoming indiffusible and immobile, as shown in Fig. 3(a).

3.2 Temperature dependence of dynamic diffusion and adsorption capacity

Figure 5 shows the changes of D_z value as a function of temperature. The D_z

values of pure CH_2O, CO, and H_2O increased in the low temperature range (< 200 K) and decreased above the temperature of 400 K. The changes of the D_z value below the low temperature limit (< 200 K) reflect the fact that molecular diffusivity in solid- or like-liquid states is inferior to that in the gaseous state. In the high temperature range (≥ 400 K), the D_z values decrease with increasing temperature, which contradicts the belief that diffusivity increases with temperature. This phenomenon can be ascribed to the z-directional diffusion motions (i.e., perpendicular to the slit walls) being confined to the nanoslit. Since the average kinetic energy of gaseous molecules is proportional to the absolute temperature, high-kinetic-energy molecules colliding with the slit walls may cause the molecules themselves to rebound from the wall and make other molecules desorb, and therefore increase the time to diffusion equilibrium and reduce the z-directional absolute displacement value (i.e., MSD = $\left| r_{i,z}(t) - r_{i,z}(0) \right|^2$ in Eq. (10)). This mechanism is responsible for the calculated D_z values decreasing with increasing temperature above the high temperature limit. Note that this unique phenomenon does not happen for the calculations of D_x and D_y due to the confinement effect being absent for the diffusion motions parallel to the slit walls.

The systemic temperature also has a profound effect on adsorption capacity. As aforementioned, high-kinetic-energy molecules colliding with GR walls may cause the molecules themselves to rebound and make other molecules desord, therefore reducing the total adsorption amount. This fundamental mechanism leads to N_{sa} decreasing with increasing systemic temperature, as shown in Fig. 6. According to the kinetic theory and the Maxwell-Boltzmann distribution function, the average particle velocity (v) and impingement rate (Γ, the rate at which gas molecules collide with the GR surface) increase with temperature as follows:[49]

$$v = \sqrt{(8\kappa T / \pi m)} \tag{11}$$

and

$$\Gamma = n\left(\frac{\kappa T}{2\pi m} \right)^{1/2} \tag{12}$$

where k is the Boltzmann's constant, T denotes the absolute temperature, and n and m

are the particle's density and mass, respectively. When the systemic temperature is increased from room temperature to 600 K, the values of v and Γ increase about 41.4% according to Eqs. (11) and (12). The sharp increases in v and Γ reflect that the adsorption amounts of CH_2O, CO_2, CO, and H_2O substantially decrease by 30~50%, as shown in Fig. 6. However, the adsorbed amounts of the mixtures only slightly change with temperature due to the mixture molecules aggregating as immobile lumps. The N_{sa} values of CO and CO_2 sharply decreased above room temperature. This suggests that CO and CO_2 are suitable to be adsorbed in the low temperature system. Moreover, GR slits exhibited excellent adsorption performances for pure CH_2O molecules even when the temperature was up to 473 K.

3.3 Effect of adsorbate concentration on diffusion and adsorption properties

Figure 7 shows the z-directional self-diffusivity for pure CH_2O, CO_2, CO, and H_2O as a function of molar concentration at room temperature. The D_z values tended to increase with increasing adsorbate concentration in the low concentration range (i.e., $c_i \leq 2.45$ mol/L). For molarities larger than 2.85 mol/L for CH_2O and 2.45 mol/L for CO, the D_z values dramatically decreased. This phenomenon can be ascribed to the effect of over-saturation that resulted in blockades and a barrier to diffusion when the concentration was above a certain threshold.

Figure 8 shows adsorption isotherms for CH_2O, CO_2, CO, and H_2O adsorbed on GR surfaces at 293 K. The adsorption isotherm shows the overall weight of the adsorbed molecules as a function of concentrations. As shown, the adsorption isotherms of CH_2O and CO_2 increase linearly with concentration, with the former increasing more sharply than the latter. This divergence resulted from the stacking regimes in adsorption. Firstly, the suspended CH_2O and CO_2 molecules were adsorbed to the vacant sites of the first adsorption layer due to strong short-range attractions arising from GR walls. With increasing concentration, the excess CH_2O molecules rapidly adsorbed and piled up, creating a second adsorption layer, but the CO_2 were lastingly to pack the first adsorption monolayer even the concentration increased continuously. Because CO_2 molecules have strong attractions between

themselves and the long-range CO_2-GR interactions are very weak, a large number of CO_2 molecules did not adsorb to GR, but instead aggregated as clusters suspended in the slit space. The adsorption characteristics of H_2O and CO are much different from those of CH_2O and CO_2. They formed uneven piled structures before the first adsorption layer was fully occupied (Fig. 1(c) and (d)). In the low-concentration limit shown in Fig. 8, the sharp rise in the adsorption isotherm of water resulted from the hydrophilicity of the GR surface and the formation of multilayer condensation. In the high concentration range, the number of adsorbed H_2O molecules increased slowly with concentration up to a saturation value, which is due to water molecules forming stable H-bonded molecular chains and small capillaries across the slit space. Moreover, the adsorption behaviors of CO were analogous to those of the Langmuir monolayer. The first CO adsorption layer weakly attracted a few free CO molecules that were short-lived and easily dissociated, causing the isotherm of CO to be much lower than those of CH_2O, CO_2, and H_2O.

3.4 Effect of constituent concentration of mixtures

The constituent concentration and composition ratio can significantly impact on the physical and chemical properties of a mixture. The fundamental properties of mixtures are required to enhance their separability and adsorbable nature. To evaluate the influences of each constituent on the adsorption behavior, mixtures with 13 different composition ratios were systematically examined, as listed in Table 4. The changes of D_Z and average binding energy ($\left|E_{b,avg}^{molecule}\right|$) of mixtures as a function of composition ratio are shown in Figs. 9 and 10, respectively. In the figures, the labels symbols of c1, c2,…, and c13 represent the simulation results for cases 1 to 13, respectively. The simulation results show that the composition ratios greatly affects the D_Z value of the mixtures. When a high-self-diffusivity constituent of the mixture was increased, the D_Z value increased. For example, when the CH_2O ratio was increased from 6.25% to 25%, the D_Z increased from 0.18 to 0.47 ($\times$ 10^{-9} $m^2 \cdot s^{-1}$). In contrast, the D_Z value decreased when the low-self-diffusivity constituent was

increased. For example, when the CO_2 ratio was increased from 6.25% to 25%, the D_Z value decreased from 0.57 to 0.47 ($\times$ 10^{-9} $m^2 \cdot s^{-1}$). Moreover, the D_Z values of all mixtures were substantially lower (by about one order of magnitude) compared to those of the pure (single-constituent) adsorbates. This is mostly due to the aggregation effect of the moleculer accumulations and the self-assembly of hydration clusters.

Figure 10 shows the average binding energy of mixtures ($\left|E_{b,avg}^{molecule}\right|$) as a function of the composition ratio. The value of $\left|E_{b,avg}^{molecule}\right|$ represents an average value of binding energy for the molecules in static adsorption on GR surfaces. As shown in Table 5, the value of $\left|E_{b,avg}^{molecule}\right|$ is slightly less than that of the first adsorption monolayer (i.e., $\left|E_{mon}^{molecule}\right|$). CO_2 has the highest binding energy at the first adsorption monolayer on GR surfaces, i.e., $\left|E_{mon}^{molecule}\right| \sim 3.99$ kcal/mol, which is consistant with the calculation of DFT/CC [30] (3.94 kcal/mol). The $\left|E_{mon}^{molecule}\right|$ value of CH_2O is 3.49 kcal/mol. The $\left|E_{mon}^{molecule}\right|$ value of the water monolayer on the GR surface is 2.67 kcal/mol, which agrees very well with the experimental and numerical results given by Rubes et al.,[50] Hamada,[51] Voloshina et al.,[52] and Suzuki et al.[53] CO has the lowest binding energy on the GR surface (~2.01 kcal/mol), and thus has the lowest adsorption isotherm and highest diffusivity. The properties of the pure components dominated the average binding energy of the mixtures. Briefly, the average binding energy of the mixtures increased with increasing composition ratio of CO_2 and CH_2O, but decreased with increasing composition ratio of CO, as shown in Fig. 10. Waters had an anomalous effect on the binding energy of the mixtures, which is primarily ascribed to three mechanisms: (i) formaldehyde was hydrated with water in the form of hydrate methanediol clusters, (ii) water randomly formed uneven multilayer condensations and capillaries before the first adsorption layer was fully occupied, and (iii) water has strong H-bonded networks and the ability to continually break and reform steady H-bonds, enabling it to be distributed non-uniformly in the GR slit.

Consequently, the coupled effect of the above-mentioned mechanisms made the absorption of the mixtures irregularly change with the water composition ratio.

4. Summary and concluding remarks

The dynamic behavior and interaction mechanism for multi-component liquid-vapor mixtures adsorbed on GR slits were investigated using atomistic simulations. The effect of interactions between the components, especially the hydration reaction between CH_2O and water, was systemically examined. The formation of hydrate methanediol clusters results in highly diffusive CH_2O and H_2O molecules becoming indiffusible and immobile. Consequently, the adsorbed amount and self-diffusivity of the mixtures were substantially lower compared to those of the pure (single-constituent) adsorbates. Moreover, most water molecules reacted with CH_2O, forming hydrate methanediol clusters, rather than dissolving CO_2 to form carbonic acid. Because the cohesion in hydrate methanediol clusters is much higher than the adhesion between clusters and the GR surface, the hydrated methanediol clusters are hydrophobic, exhibiting a large contact angle on graphitic surfaces. This result supports the findings of Li *et al*[6] who reported that exposure to air-born hydrocarbons and contaminants made GR surfaces hydrophobic. Moreover, the GR slits exhibited excellent adsorption ability for pure CH_2O molecules, even when the temperature was up to 473 K. CH_2O can thus be efficiently captured in low-moisture and high-concentration operation conditions. The water possesses strong H-bonded networks and can continuously reform steady H-bonds, it randomly formed uneven multilayer condensations and capillary distributions in the GR slit. The hydrations had an irregular effect on the adsorption properties of the mixtures, which is disadvantageous for the capture and separation of a particular component from the mixture. Since the long-range CO_2-GR and CO-GR attractions are quite weak, only the CO_2 and CO molecules close to the GR walls could be adsorbed. Moreover, the adsorbed amounts of CO and CO_2 are sharply reduced at above room temperature. These results indicate that CO and CO_2 are suitable for capture in narrow pores at low temperatures.

Acknowledgements

References

[1] C. Sanchez, K. J. Shea, S. Kitagawa, *Chem. Soc. Rev.*, 2011, **40**, 550–562.

[2] J. J. Magda, M. Tirrell, H. T. Davis, J. Chem. *Phys.*, 1985, **83**, 1888-1901.

[3] A. Kapoor, R. T. Yang, *Chem. Eng. Sci.*, 1989, **44**, 1727-1733.

[4] Y. C. Wang, S. P. Ju, Phys. *Chem. Chem. Phys.*, 2011, **13**, 1323-1331.

[5] A. V. Shevade, S. Jiang, K. E. Gubbins, *J. Chem. Phys.*, 2000, **113**, 6933.

[6] Z. Li, Y. Wang, A. Kozbial, G. Shenoy, F. Zhou, R. McGinley,P. Ireland, B. Morganstein, A. Kunkel, S. P. Surwade, L. Li, H. Liu, *Nat. Mater.*,2013, **12**, 925-931.

[7] A. K. Winkler, N. S. Holmes, J. N. Crowley, *Phys. Chem. Chem. Phys.*, 2002, **21**, 5270-5275.

[8] M. Heuchel, G. M. Davies , E. Buss ,N. A. Seaton, *Langmuir*, 1999, **15**, 8695-8705.

[9] A. Vishnyakov, P. I. Ravikovitch, A. V. Neimark, *Langmuir*, 1999**, 15***, 8736-8742.

[10]V. Ballenegger, S. Picaud, C. Toubin, *Chem. Phys. Lett.*, 2006, **432**, 78-83.

[11]B. Collignon, S. Picaud, *Chem. Phys. Lett.*, 2004, **393**, 457-463.

[12]S. K. Bhatia, K. Tran, T. X. Nguyen, D. Nicholson, *Langmuir*, 2004, **20**, 9612-9620.

[13]B. Liu, B. Smit, *J. Phys. Chem. C*, 2010**, 114**, 8515–8522

[14]C. Liu, T. R. Cundari, A. K. Wilson, *J. Phys. Chem. C*, 2012, **116**, 5681-5688.

[15] I. Skarmoutsos, G. Tamiolakis, G. E. Froudakis, *Phys. Chem. Chem. Phys.*, 2014, **16**, 876-879.

[16] J. Zhou, W. Wang, *Langmuir,* 2000, **16***,* 8063-8070.

[17] M. Levitt, M. Hirshberg, R. Sharon , V. Daggett, *Comput. Phys. Commun.*, 1995, **91**, 215-231.

[18] M. Levitt, M. Hirshberg, R. Sharon, K. E. Laidig, V. Daggett, *J. Phys. Chem. B,* 1997, **101***,* 5051-5061.

[19] T. Werder, J. H. Walther, R. L. Jaffe, T. Halicioglu, P. Koumoutsakos, *J. Phys. Chem. B*, 2003, **107**, 1345-1352.

[20] S. Pałucha, Z. Gburski, J. Biesiada, *J. Mol. Struct.*, 2004, **704**, 269-273.

[21] A. Alexiadis, S. Kassinos, *Chem. Phys. Lett.*, 2008, **460**, 512-516.

[22] R. M. Levy, D. B. Kitchen, J. T. Blair, K. K. Jespersen, *J . Phys. Chem.*, 1990, **94**, 4410-4416.

[23] W. L. Jorgensen, D. S. Maxwell, J. T. Rives, *J. Am. Chem. Soc.* 1996, **118***,* 11225-11236.

[24] J. M. Haile, *Molecular dynamics simulation: elementary methods*, Wiley-Interscience, New York, 1997.

[25] P. H. Hang, *Compos. Sci. Technol.*, 2012, **72**, 599-607.

[26] J. K. Kuo, P. H. Huang, W. T. Wu, C. M. Lu, *Appl. Phys. A.*, 2014, **114**, 1247-1256.

[27] J. H. Walther, T. Werder, R. L. Jaffe, P. Gonnet, M. Bergdorf, U. Zimmerli, P. Koumoutsakos, *Phys. Chem. Chem. Phys.*, 2004, **6**, 1988-1995.

[28] M. E. Schrader, J. Phys. Chem., 1975, 79(23), 2508-2515.

[29] I. Morcos, J. Chem. Phys., 1972, 57(4), 1808-1802.

[30] M. E. Tadros, P. Hu and A. W. Adamson, J. Colloid Interface Sci., 1974, 49(2), 184-195.

[31] M. E. Schrader, J. Phys. Chem., 1980, 84, 2774–2779.

[32] J. Rafiee, X. Mi, H. Gullapalli, A. V. Thomas, F. Yavari, Y. Shi, P. M. Ajayan, N. A. Koratkar, *Nature Mater.*, 2012, **11**, 217-222.

[33] G. Scocchi, D. Sergi, C. D'Angelo, A. Ortona, *Phys. Rev. E*, 2011, **84**, 061602-1-8.

[34] F. Taherian, V. Marcon, N. F. A. van der Vegt, *Langmuir*, 2013, **29**, 1457-1465.

[35] T. Werder, J. H. Walther, R. L. Jaffe, T. Halicioglu, P. Koumoutsakos, *J. Phys. Chem. B*, 2003, **107**, 1345-1352.

[36] R. L. Jaffe, P. Gonnet, T. Werder, J. H. Walther, P. Koumoutsakos, *Mol. Simul.*, 2004, **30(4)**, 205-216.

[37] M. Lundgren, N. L. Allan, T. Cosgrove, *Langmuir*, 2002, **18(26)**, 10462.10466.

[38] R. F. Cracknell, D. Nicholson, K. E. Gubbinst, *J. Chem. Soc.*, 1995, **91**, 1377-1383.

[39] M. Holz, S. R. Heil, A. Sacco, *Phys. Chem. Chem. Phys.*, 2000, **2**, 4740-4742.

[40] Z. C. Kramer, K. Takahashi, V. Vaida, R. T. Skodje, *J. Chem. Phys.*, 2004, **136**, 164302-1-9.

[41] A. D. Kulkarni, V. Ganesh, S. R. Gadre, *J. Chem. Phys.*, 2004, **121**, 5043-5050.

[42] S. Morooka, N. Matubayasi, M. Nakahara, *J. Phys. Chem.* A, 2007, **111**, 2697-2705.

[43] C. Mihesan, N. Lebrun, M. Ziskind, B. Chazallon, C. Focsa, J. L. Destombes, *Surf. Sci.*, 2004, **566-568**, 650-658.

[44] C. Focsa, C. Mihesan, M. Ziskind, B. Chazallon, E. Therssen, P. Desgroux, J. L. Destombes, *J. Phys.: Condens. Matter.*, 2006, **18**, S1357-S1387.

[45] M. Ziskind, C. Mihesan, N. Lebrun, B. Chazallon, C. Focsa, J. L. Destombes, Appl. Phys. A-Mater. Sci. Process., 2004, **79**, 991-995.

[46] N. Lebrun, P. Dhamelincourt, C. Focsa, B. Chazallon, J. L. Destombes, D. Prevost, 2003, *J. Raman Spectrosc.*, **34**, 459-464.

[47] B. Chazallon, N. Lebrun, P. Dhamelincourt, C. Toubin, C. Focsa, *J. Phys. Chem. B*, 2005, **109**, 432-439.

[48] J. B. Hudson, *Surface science: An introduction,* Wiley-Interscience, New York, 1998.

[49] M. Rubes, J. Kysilka, P. Nachtigall, O. Bludsky, *Phys. Chem. Chem. Phys.*, 2010, **12**, 6438-6444.

[50] I. Hamada, *Phys. Rev. B*, 2012, **86**, 195436.

[51] E. Voloshina, D. Usvyat, M. Schutz, Y. Dedkov, B. Paulus, *Phys. Chem. Chem. Phys.*, 2011, **13**, 12041-12047.

[52] S. Suzuki, P. G. Green, R. E. Bumgarner, S. Dasgupta, W. A. Goddard III, G. A. Blake, *Science*, 1992, **257**, 942-945**.**

Tables

Table 1. Bond length energy and bond angle energy for H_2O, CO_2, CO, and CH_2O molecules.

Parameter	k_b^i (kcal/mol·Å^{-2})	b_0^i (Å)	k_θ^i (kcal/mol·rad^{-2})	θ_0^i (deg)
(O-H)$_{H_2O}$	250	1.0	60	109.47
(C-O)$_{CO_2}$	5000	1.163	5000	180
(C-O)$_{CO}$	5000	1.128	–	–
(C-H)$_{CH_2O}$	250	1.1006	60	116.52
(C-O)$_{CH_2O}$	250	1.203	60	121.74

Table 2. Nonbonded energy parameters of F3C model for water-water interactions.

	r_0(Å)	ε (kcal/mol)	q (e)
O$_{H_2O}$	3.55322	0.18479	-0.82
H$_{H_2O}$	0.9	0.01	0.41

Table 3. Intermolecular potential parameters for Lennard-Jones and Coulomb interactions.

	r_0(Å)	ε (kJ/mol)	q (e)
C$_{graphite}$[5]	3.4	0.2328	0
C$_{CO_2}$[21]	2.7918	0.23982	0.5888
O$_{CO_2}$[21]	3.0	0.68722	-0.2944
H$_{H_2O}$[19]	0	0	0.41
O$_{H_2O}$[19]	3.166	0.65017	-0.82
C$_{CO}$[20]	3.55	0.3089	0.0223
O$_{CO}$[20]	2.95	0.512	-0.0223
C$_{CH_2O}$[22-23]	3.75	0.43852	0.45
H$_{CH_2O}$[22-23]	2.42	0.06262	0
O$_{CH_2O}$[22-23]	2.96	0.87712	-0.45

Table 4. List of constituent ratios of multi-component mixtures used in simulations.

Composition	CO_2 (%)	CO (%)	CH_2O (%)	H_2O (%)
Case 1	25	25	25	25
Case 2	27.1	27.1	**18.7**	27.1
Case 3	29.07	29.07	**12.8**	29.07
Case 4	31.25	31.25	**6.25**	31.25
Case 5	27.1	27.1	27.1	**18.7**
Case 6	29.07	29.07	29.07	**12.8**
Case 7	31.25	31.25	31.25	**6.25**
Case 8	**18.7**	27.1	27.1	27.1
Case 9	**12.8**	29.07	29.07	29.07
Case 10	**6.25**	31.25	31.25	31.25
Case 11	27.1	**18.7**	27.1	27.1
Case 12	29.07	**12.8**	29.07	29.07
Case 13	31.25	**6.25**	31.25	31.25

Table 5. z-directional self-diffusivity, i.e., D_z, average values of binding energy for molecules in static adsorption, i.e., $\left|E_{b,avg}^{molecule}\right|$, and binding energy at first adsorption monolayer, i.e., $\left|E_{mon}^{molecule}\right|$, for pure CH_2O, CO_2, CO, H_2O, and an equivalent fraction mixtures (MIX). Simulations were performed with c_i = 3.38 mol/L and d = 48.84 Å at room temperature.

	CO_2	CO	CH_2O	H_2O	MIX
D_z (10^{-9} m^2/s)	2.21	12.13	16.11	15.78	0.47
$\left|E_{b,avg}^{molecule}\right|$ (kcal/mol)	-3.9401	-1.9548	-3.3705	-2.3964	-3.2224
$\left|E_{mon}^{molecule}\right|$ (kcal/mol)	-3.9889	-2.0065	-3.4889	-2.6754	-3.5439

Figures
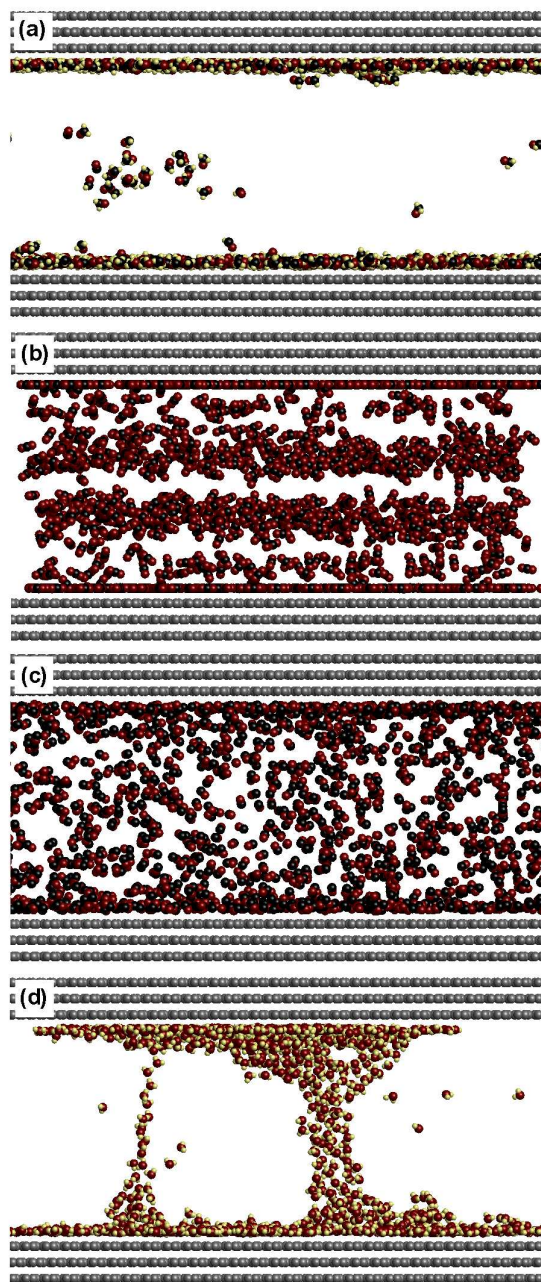
FIG. 1. Representative snapshots of MD simulation model for (a) formaldehyde, (b) carbon dioxide, (c) carbon monoxide, and (d) water molecules adsorbed to GR slits. Simulations were performed with molar concentration $c_i = 3.38$ mol/L and slit width $d = 48.84$ Å at room temperature. Large black spheres, red spheres, and small yellow spheres represent C, O, and H atoms, respectively. Gray spheres denote C atoms of GR.
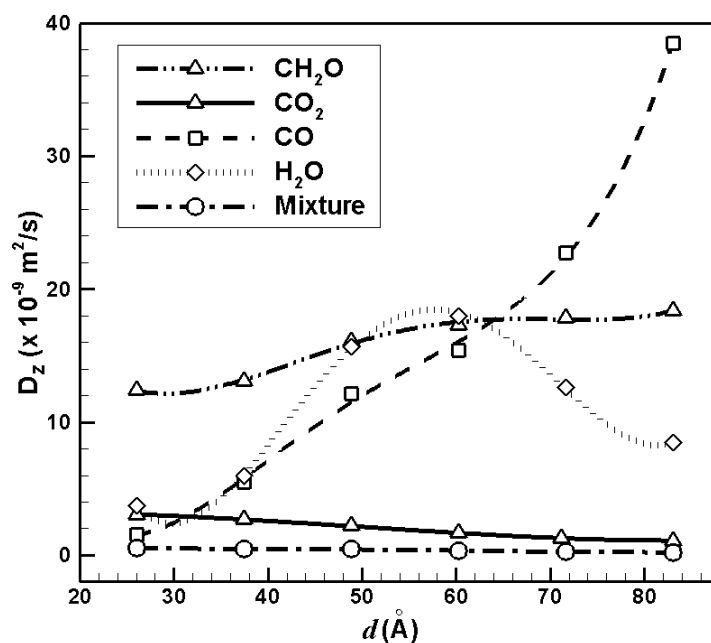
FIG. 2. z-directional self-diffusivity as function of slit width for pure CH_2O, CO_2, CO, H_2O, and their mixture. Simulations were performed with c_i = 3.38 mol/L at room temperature.
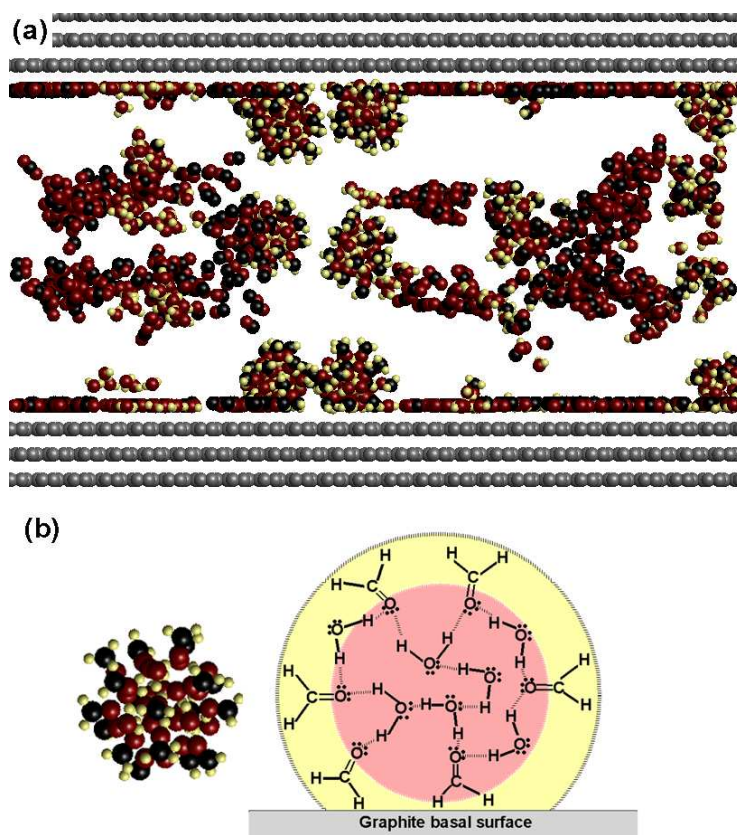
FIG. 3. (a) Adsorptive conformation of mixture comprising equivalent fractions of CH_2O, CO_2, CO, and H_2O, and (b) hydrate methanediol globular cluster (left) and corresponding self-assembled structure with H_2O in core and CH_2O on shell (right).
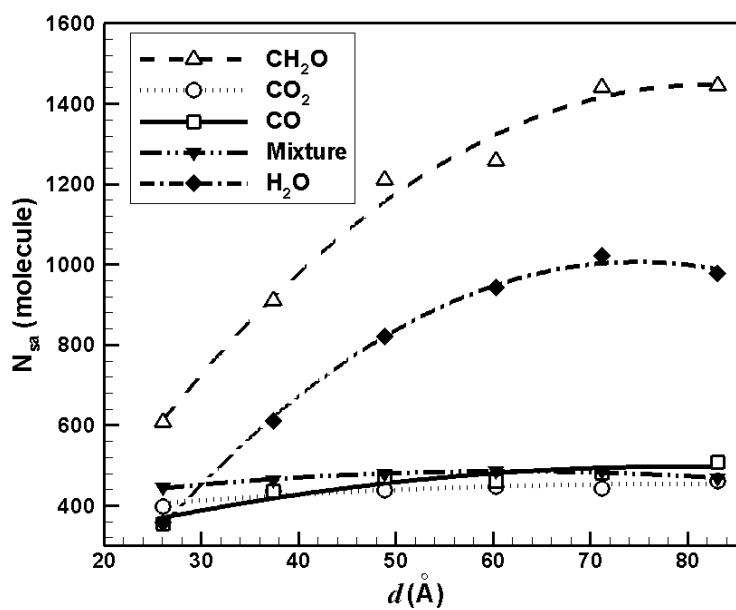
FIG. 4. Amount of static adsorption as function of slit width for pure CH_2O, CO_2, CO, H_2O, and their mixture. Simulations were performed with $c_i = 3.38$ mol/L at room temperature.
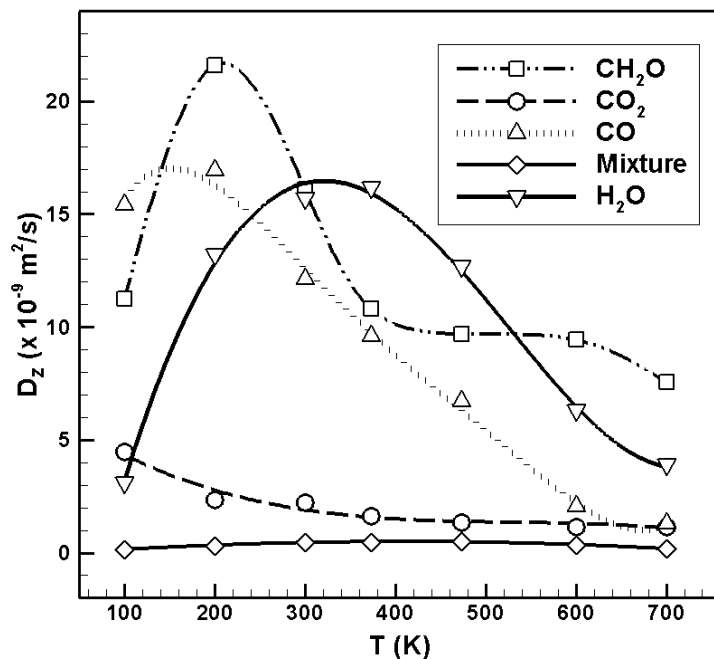
FIG. 5. *z*-directional self-diffusivity as function of temperature for pure CH_2O, CO_2, CO, H_2O, and their mixture. Simulations were performed at $c_i = 3.38$ mol/L and $d = 48.84$ nm.
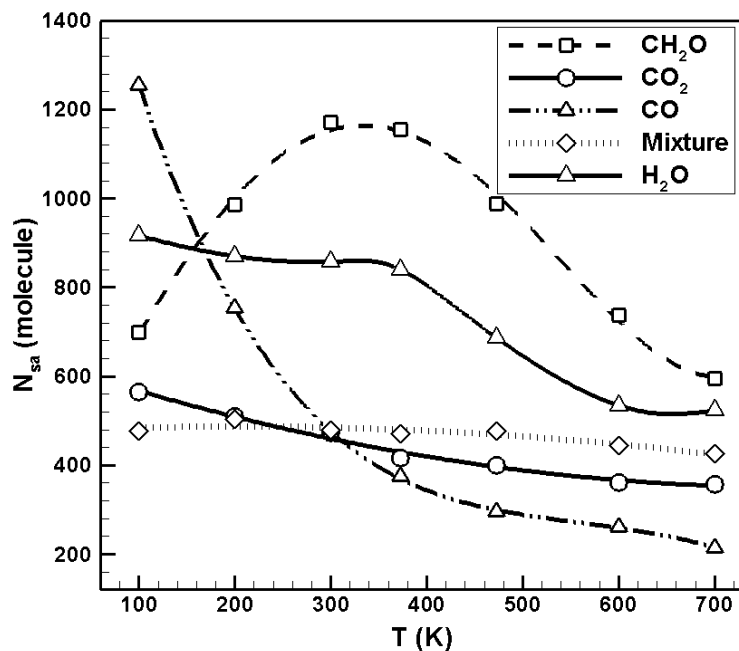
FIG. 6. Amount of static adsorption as function of temperature for pure CH_2O, CO_2, CO, H_2O, and their mixtures. Simulations were performed at $c_i = 3.38$ mol/L and $d = 48.84$ nm.
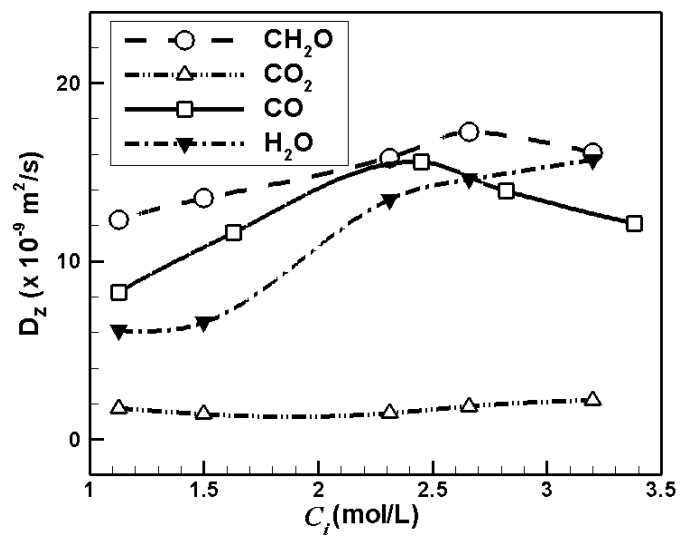
FIG. 7. *z*-directional self-diffusivity as function of molar concentration at room temperature.
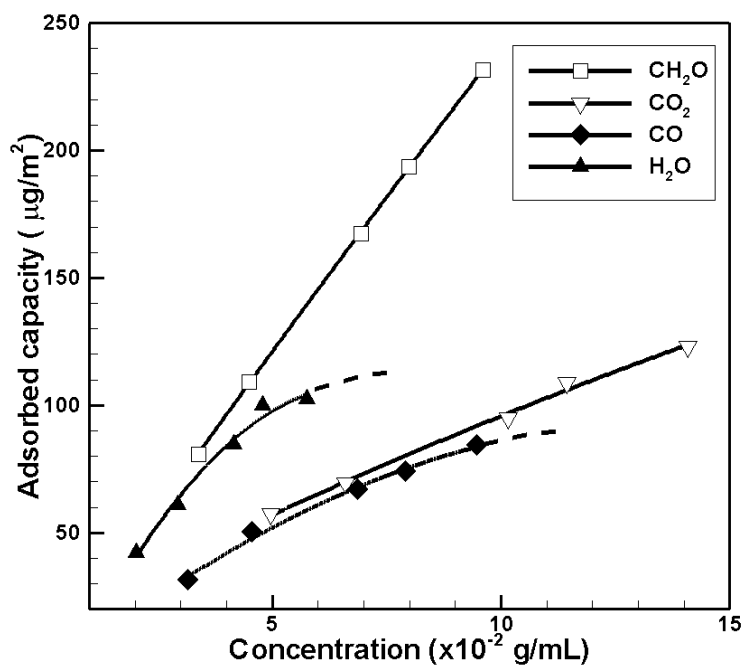
FIG. 8. Adsorption isotherms for CH_2O, CO_2, CO, and H_2O adsorbed on GR slits ($d =$ 48.84 Å) at 293 K.
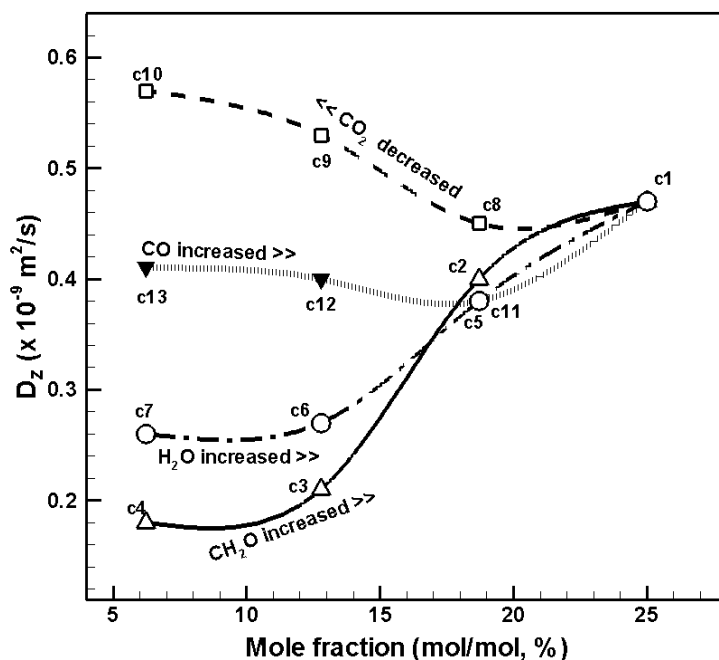
FIG. 9. *z*-directional self-diffusivity as function of mole fraction for mixtures with various composition ratios at 293 K. Labels c1, c2,…, c13 correspond to composition ratios of case 1 to 13, respectively, in Table 4 (e.g., c10 denotes the mixture of CO_2: CO: CH_2O: H_2O with 6.25%: 31.25%: 31.25%: 31.25%, and c9 denotes that with 12.8%: 29.07%: 29.07%: 29.07%). Lines show changes of D_Z with changing concentration of a certain constituent.
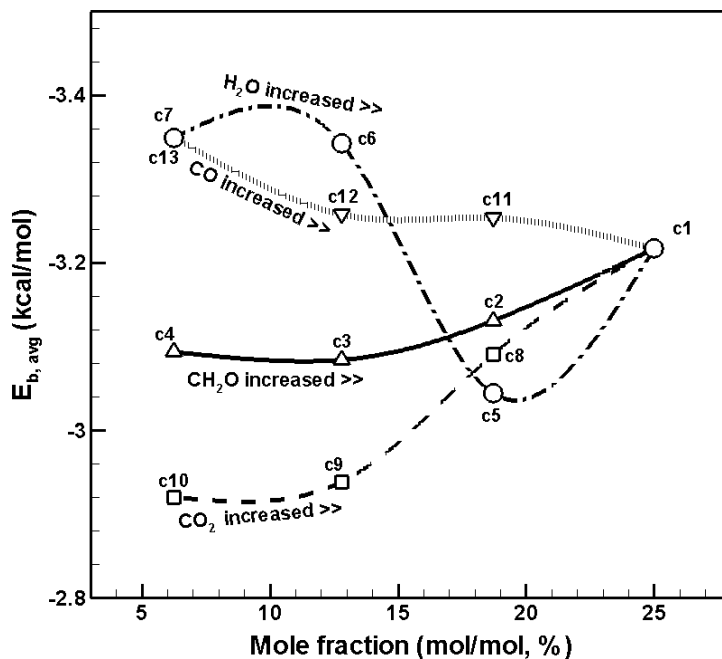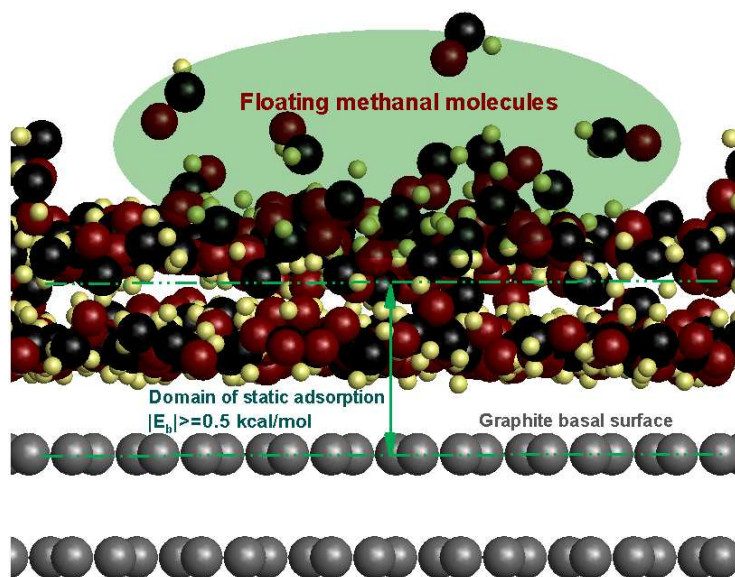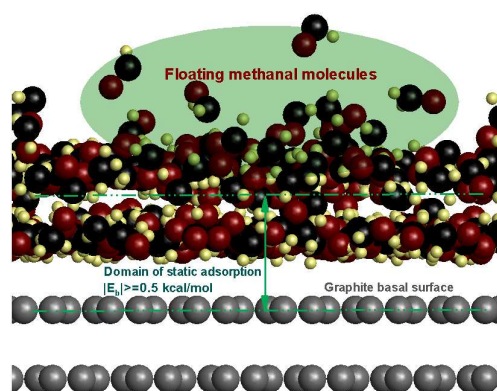
FIG. 10. Average binding energy as function of mole fraction for mixtures with various composition ratios at 293 K. c1, c2…, c13 correspond to composition ratio of case 1 to 13, respectively, in Table 4 (as in Fig. 9). Lines show changes of average binding energy with changing concentration of a certain constituent.

Graphical abstract

We report a multi-component liquid-vapor adsorption study that allowed us to predict the ideal adsorption conditions and to explore the fundamental interaction and adsorption behaviors for formaldehyde, carbon dioxide, carbon monoxide, and water mixtures in GR slit pores.

Graphical abstract

We report a multi-component liquid-vapor adsorption study that allowed us to predict the ideal adsorption conditions and to explore the fundamental interaction and adsorption behaviors for formaldehyde, carbon dioxide, carbon monoxide, and water mixtures in GR slit pores.